We are IntechOpen, the world's leading publisher of Open Access books Built by scientists, for scientists

4,800
Open access books available

122,000
International authors and editors

135M
Downloads

Our authors are among the

154
Countries delivered to

TOP 1%
most cited scientists

12.2%
Contributors from top 500 universities

CLARIVATE ANALYTICS BOOK CITATION INDEX INDEXED

WEB OF SCIENCE™

Selection of our books indexed in the Book Citation Index in Web of Science™ Core Collection (BKCI)

Interested in publishing with us?
Contact book.department@intechopen.com

Numbers displayed above are based on latest data collected.
For more information visit www.intechopen.com

24

Wave Velocity Dispersion and Attenuation in Media Exhibiting Internal Oscillations

Marcel Frehner[1], Holger Steeb[2] and Stefan M. Schmalholz[3]
[1]*Department for Geodynamics and Sedimentology, University of Vienna,*
[2]*Mechanics - Continuum Mechanics, Ruhr-University Bochum,*
[3]*Geological Institute, ETH Zurich,*
[1]*Austria*
[2]*Germany*
[3]*Switzerland*

1. Introduction

Modeling the propagation of acoustic or fully elastic (i.e. seismic) waves is an important tool for interpreting, understanding and predicting real-world measurements in various industrial disciplines. In this context, modeling can be anything from three-dimensional full waveform modeling using numerical techniques (e.g. finite difference method, finite element method, spectral method; Kelly & Marfurt, 1990; Martin & Komatitsch, 2009) to analytical treatment of wave phenomena (e.g. Liu et al., 2000; Aki & Richards, 2002; Korneev, 2008) and can be in both, time and frequency domain. In its simplest form, the propagation of waves through a heterogeneous medium is described with a linear elastic material behavior (Aki & Richards, 2002). Such models, including and resolving heterogeneities on various scales with different elastic material parameters, are already able to describe a number of wave propagation phenomena, e.g. reflection and transmission coefficients at interfaces, scattering at heterogeneities (Frehner et al., 2008) or propagation of surface waves. As the number of investigated heterogeneities increases, the complexity of the numerical model and the computational cost also increases. For example, Saenger et al. (2007) use an advanced parallel finite difference scheme to model wave propagation on the pore-scale resolving the entire pore structure of a rock or Lee et al. (2009) use a spectral element method comprising an unstructured numerical mesh to investigate the effect of topography on seismic wave amplitudes. These are only two examples of a numerical model with a basic linear elastic constitutive equation containing a large number of heterogeneities with very complex geometries.

When the number of heterogeneities and therefore the geometrical complexity of a model becomes too large and/or the characteristic size of the heterogeneities is much smaller than the wavelength under consideration, effective medium theories are applied. Such models upscale physical processes on the microscale (i.e. much smaller than the wavelength) by introducing coarse-grained/homogenized macroscopic effective material parameters. For example, Korneev et al. (2004) added an additional term describing viscous damping to the elastic wave equation to take into account attenuation. However, the physical process acting

Source: Wave Propagation in Materials for Modern Applications, Book edited by: Andrey Petrin,
ISBN 978-953-7619-65-7, pp. 526, January 2010, INTECH, Croatia, downloaded from SCIYO.COM

on the microscale causing the attenuation is not described. The widely accepted effective medium model for fully saturated porous media is the Biot model (Biot, 1962). More advanced models for partially saturated porous media can be separated into two groups: (1) models based on Biot's theory for fully saturated media, but applying spatially varying pore fluid properties representing a partial saturation on the mesoscale (i.e. larger than the pore size and smaller than the wavelength under consideration; White, 1975; Dutta & Ode, 1979; Quintal et al., 2009) and (2) macroscale effective medium models for three-phase media (i.e. solid rock, wetting and non-wetting fluid) considering a homogenized partial saturation on the pore-scale, including in particular capillary pressure effects (Santos et al., 1990; Smeulders & van Dongen, 1997; Wei & Muraleetharan, 2002). Common to all of these effective medium models for fully or partially saturated porous rocks is that in their derivation the individual phases are usually mixed and the material properties are averaged over a so-called representative elementary volume. By doing so, processes taking place at the interfaces between the individual phases (e.g. surface tension effects or scattering at the pore structure) are ignored. More advanced mixture theory-based models, which take specific surface areas between wetting and non-wetting phases into account, are still limited to quasi-static processes. However, such effects can be re-included by introducing additional effective material parameters.

Within a medium containing any kind of heterogeneity or a number of heterogeneities, oscillations with a characteristic resonance frequency, depending on the mass and internal length of the heterogeneity, can occur. When excited, heterogeneities can self-oscillate with their natural frequency (Carstensen & Foldy, 1947; MacPherson, 1957; van Wijngaarden, 1972; Anderson & Hampton, 1980). If the external excitation force is an acoustic or seismic wave, this process is called resonant scattering (Werby & Gaunaurd, 1990; Hassan & Nagy, 1997) and has application in non-destructive testing of materials (e.g. Schultz et al., 2006). Korneev (2009) even demonstrated that the resonance frequency of an object in the subsurface with a large impedance contrast to its surrounding can be measured with an active seismic experiment at the Earth surface. The oscillations are more easily detectable in late arrivals when they are not masked by high-energy body waves. Other mechanisms can cause oscillations within a heterogeneous medium. For example, the dynamical behavior of non-wetting fluid blobs or fluid patches in idealized residually saturated pore spaces were studied (Dvorkin et al., 1990; Graham & Higdon, 2000a; Graham & Higdon, 2000b). Thereby, one of the main results is the oscillatory movement of the fluids when an external driving force is applied (Hilpert et al., 2000). The restoring force driving the oscillations is the surface tension force or capillary force. The fact that isolated oil blobs in residually saturated pore spaces can exhibit a resonance frequency, motivated the suggestion of a new enhanced oil recovery method (EOR) termed "wave stimulation of oil" or "vibratory mobilization" (Beresnev & Johnson, 1994; Iassonov & Beresnev, 2003; Beresnev et al., 2005; Li et al., 2005; Hilpert, 2007; Pride et al., 2008). Another example of oscillatory behavior within a medium is given by Urquizu and Correig (2004). They showed that under certain circumstances a seismic wave pulse propagating through a layered medium can be described mathematically with a differential equation for an oscillator.

All of these oscillatory phenomena within a medium should have an effect on acoustic or seismic waves propagating through such a heterogeneous medium. Presumably, the wave will show a strongly frequency-dependent propagation behavior (i.e. velocity dispersion

and frequency-dependent attenuation). However, such oscillatory phenomena are not included in current effective medium theories, such as the Biot theory (Biot, 1962). Oscillations are usually described on the microscale (i.e. the scale of one single oscillator; Dvorkin et al., 1990; Graham & Higdon, 2000; Hilpert et al., 2000; Beresnev et al., 2005), not taking into account the macroscale, i.e. continuous scale. Frehner et al. (2009) presented a model to combine the dynamics of wave propagation and rock-internal oscillations caused by capillarity effects using an effective medium theory. However, the model was presented for internal undamped oscillations with only one particular resonance frequency.

In this chapter, we extend the effective medium model of Frehner et al. (2009) by introducing a viscous damping term and generalize the model for an arbitrary number of resonance frequencies (described e.g. by a probability density function of possible resonance frequencies in the limit case). We describe the simplified case of an acoustic medium exhibiting internal oscillations, i.e. a linear elastic medium with an elastic shear modulus equal to zero. In such a material only one type of wave (i.e. a compressional wave or P-wave) can propagate. The internal oscillations will be described by the equation of motion for a damped harmonic oscillator. Different to Frehner et al. (2009), we use as an example for such a medium water containing gas bubbles, where the dispersed gas bubbles can oscillate with their natural frequency. For that specific example, the elastic and viscous interaction forces between the phases can be derived analytically and a comparison with literature and experimentally obtained results can be performed.

2. Mathematical model of acoustic medium exhibiting internal oscillations

For simplicity reasons and because we want to understand first-order effects, we choose a basic model. By choosing an acoustic medium, we concentrate on only one type of wave (i.e. a compressional wave or P-wave, also called acoustic wave or sound wave). Because only one type of wave can propagate in an acoustic medium, we choose a one-dimensional model description (x is the spatial coordinate). Thus, we neglect amplitude decrease of the acoustic wave due to geometrical spreading and energy redirection in the different spatial directions.

The chosen model leads to a straightforward analogy, i.e. water (the acoustic medium) containing gas bubbles (internal oscillations). This particular case was studied by a number of researchers (e.g. Minnaert, 1933; Carstensen & Foldy, 1947; Fox et al., 1955; MacPherson, 1957; Silberman, 1957; van Wijngaarden, 1972; Commander & Prosperetti, 1989) and a large number of experimental data is available, as well as detailed theory. However, we choose a different approach for deriving our equations. While in the cited literature the dynamics of the bubble is considered in detail, we take the result of this work and simply assume that the bubble movement can be described by a damped harmonic oscillator. Fig. 1 shows the conceptual one-dimensional model of water (acoustic medium) containing gas bubbles (oscillators).

The governing set of equations for the gas-water-mixture can be derived by averaging the properties of the gas bubbles in a certain representative elementary volume and applying concepts of the mixture theory (Truesdell, 1957; Bowen, 1980; Bowen, 1982). In contrast to classical mixture theory, we would like to denote that only the fluid (i.e. water) phase is continuous, while the gas phase consists of individual disconnected bubbles. Therefore, no acoustic wave can propagate through the gas phase and we do not introduce a Darcy-like term to describe the flow of the gas phase.

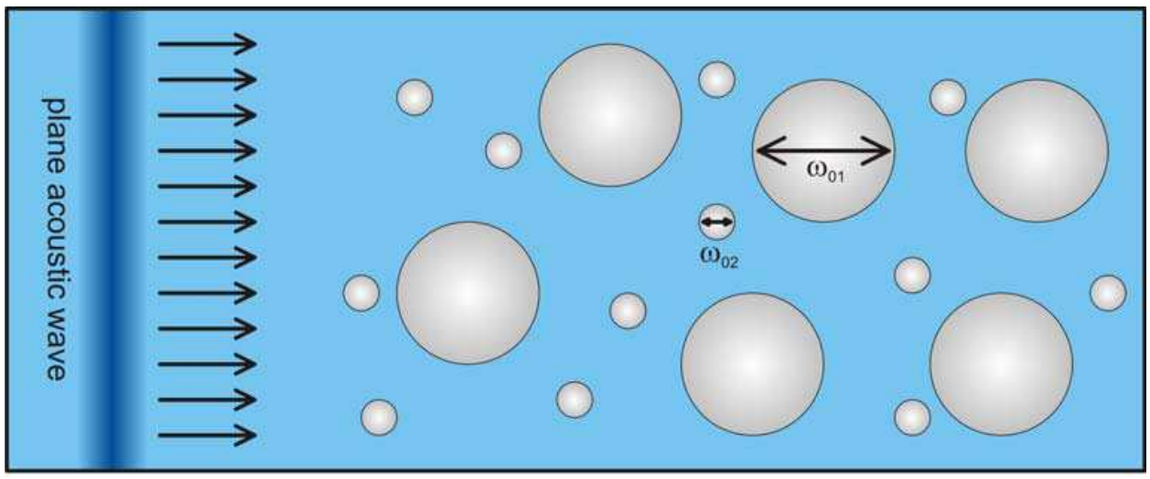

Fig. 1. Conceptual one-dimensional model of an acoustic medium (i.e. water) exhibiting internal oscillations (i.e. individual disconnected and compressible gas bubbles). Exemplarily, a model with two different internal resonance frequencies (ω_1 and ω_2) is displayed here. Only displacements and waves propagating in the horizontal (i.e. x-) direction are considered.

2.1 Oscillations of gas bubbles

First, we study the oscillatory behavior of one individual disconnected gas bubble (superscript g) in water (superscript f). Minnaert (1933) determined the angular eigenfrequency of a spherical gas bubble in water under isothermal conditions as

$$\Omega_{0j} = \frac{1}{r_j}\sqrt{\frac{3\gamma p_0}{\rho^{fR}}}\,, \tag{1}$$

depending on the radius r_j of the bubble, the heat capacity ratio γ of the gas, the initial gas pressure in the bubble p_0 and the density of bubble-free water ρ^{fR}. The index j denotes the particular bubble size under consideration. Superscript R denotes material parameters of a single-phase medium (i.e. bubble free water or pure gas). The initial gas pressure in the bubble p_0 is assumed to be the same for all bubble sizes and can be calculated from the water depth H as

$$p_0 = 10^5 + 9.81\rho^{fR}H\,. \tag{2}$$

The value 10^5 [Pa] is the atmospheric pressure at sea level, i.e. the pressure at the water surface. The value 9.81 [m/s²] is the gravitational acceleration. Because we do not follow the derivations of Minnaert (1933) and we couple the bubble oscillations to a wave propagation equation, we can not expect the resonance frequency of our coupled wave propagation-oscillator model to be equal to Equation (1). However, we use the frequency of Minnaert (1933) (Equation (1)) as a reference frequency. Accordingly, the resonance frequency of our model is

$$\omega_{0j} = A\Omega_{0j}\,. \tag{3}$$

The scaling factor A will be determined, once the coupled system of equations is derived further down. According to the harmonic oscillator model, the restoring force for one oscillating gas bubble is

$$\hat{f}_j^g = -\hat{m}_j^g \omega_{0j}^2 w \,, \tag{4}$$

where $\hat{m}_j^g$ is the mass of one individual gas bubble with radius r_j and $w = u_j^g - u^f$ is the relative displacement of the center of mass of the gas bubble to the fluid (with u being displacement). The symbol ^ above parameters refers to the fact that Equation (4) is valid for one particular isolated gas bubble, i.e. at one particular position in the model, and is not a continuous formulation for the whole model yet. According to Batchelor (2000), the viscous interaction (i.e. damping) force of a single gas bubble surrounded by a viscous fluid is given by

$$\hat{b}_j^g = -4\pi r_j \eta^{fR} \dot{w} \,, \tag{5}$$

where η^{fR} is the dynamic viscosity of bubble-free water and $\dot{w}$ is the material time derivative of the relative displacement w, i.e. the relative velocity of the center of mass of the gas bubble to the fluid[1]. Note that the interacting forces (Equations (4) and (5)) are written in terms of relative displacement and velocity. We would like to remark, that, in contrast to Biot-type models or other mixture theory-based models, two physically different momentum interaction terms are introduced. A purely elastic term of oscillatory nature that scales with the volume of the bubble and a viscous term that scales with the specific surface of the bubble. Thus we are able to take into account damping with respect to the specific surface area of the gas bubbles.

The volume of one single gas bubble of radius r_j is given by $\hat{V}_j^g$ while the number n_j is introduced as the number of bubbles with the same radius r_j per representative elementary volume (REV), i.e. n_j carries the dimension [1/m^3]. Finally, in order to describe the macroscopic behaviour of the gas-fluid-mixture in the REV, we introduce the volume fraction of the sum of gas bubbles with radius r_j as ϕ_j^g. Summing up all bubbles with different radii in the REV is done by summing up the volume fractions ϕ_j^g of bubbles with radius r_j. The result is the overall volume fraction of the gas phase ϕ^g. The following relations apply:

---

[1]The non-equilibrium interaction between the fluid and the gas bubble was generalized in Batchelor (2000) for bubbles consisting of fluids with an intrinsic viscosity leading to

$$\hat{f}_j^g = -4\pi r_j \eta^{fR} \frac{\eta^{fR} + \frac{3}{2}\eta^{gR}}{\eta^{fR} + \eta^{gR}} \dot{\hat{w}}$$

with the limits for

a) gas bubbles: $\lim \hat{f}_j^g \Big|_{\eta^{gR} \to 0} = -4\pi r_j \eta^{fR} \dot{\hat{w}}$

b) rigid spheres $\lim \hat{f}_j^g \Big|_{\eta^{gR} \to \infty} = -6\pi r_j \eta^{fR} \dot{\hat{w}}$

$$\phi_j^g = n_j \hat{V}_j^g \qquad \text{and} \qquad \phi^g = \sum_{j=1}^{m} \phi_j^g = \sum_{j=1}^{m} \left(n_j \hat{V}_j^g \right). \tag{6}$$

The value m is the number of different gas bubble sizes in the system. For example, in a model containing a large number of equally sized gas bubbles, m is equal to 1, in contrast to n_1, which is the absolute number of gas bubbles with that particular size. Also, partial densities ρ_j^g and ρ^g are introduced as

$$\rho_j^g = n_j \hat{m}_j^g = \phi_j^g \rho^{gR} \quad \text{and} \quad \rho^g = \sum_{j=1}^{m} \left(\phi_j^g \right) \rho^{gR} = \phi^g \rho^{gR}. \tag{7}$$

The partial density ρ_j^g is defined as the mass of gas inside gas bubbles of one particular radius r_j per REV and is therefore different to the true or so-called effective density of gas ρ^{gR}. The partial density ρ^g is defined as the total mass of gas per REV.

2.2 Acoustic medium containing oscillating gas bubbles

The summation of all momentum interaction terms $\hat{f}_j^g$ and $\hat{b}_j^g$ of the gas phase (Equations (4) and (5)) must be equal to the momentum interaction term of the water phase. Therefore, the following constraints must be fulfilled:

$$\sum_{j=1}^{m} \left(n_j \hat{f}_j^g \right) + \sum_{j=1}^{m} \left(n_j \hat{b}_j^g \right) + f^f + b^f = 0. \tag{8}$$

The water phase is assumed to behave like a purely acoustic medium. Thus, we neglect any viscous shear stresses. The balance of momentum in one dimension is given by:

$$\rho^f \ddot{u}^f = \frac{\partial \sigma}{\partial x} + f^f + b^f. \tag{9}$$

In Equation (9), ρ^f is the partial density of water, i.e. $\rho^f = \phi^f \rho^{fR}$ (with ϕ^f and ρ^{fR} being the volume fraction and the true density of water, respectively) and σ is the normal stress in the water phase in the only spatial direction x and is defined as positive for extensional stress. The constitutive equation for the stress in the (acoustic) water phase has the following form:

$$\sigma = \phi^f K^f \frac{\partial u^f}{\partial x}. \tag{10}$$

In Equation (10), K^f is the bulk modulus of water. The balance of momentum for the water phase (Equation (9)) becomes (including Equations (4), (5), (8) and (10))

$$\rho^f \ddot{u}^f = \phi^f K^f \frac{\partial^2 u^f}{\partial x^2} + \sum_{j=1}^{m} \left(n_j \hat{m}_j^g \omega_{0j}^2 \left(u_j^g - u^f \right) \right) + \sum_{j=1}^{m} \left(4\pi n_j r_j \eta^{fR} \left(\dot{u}_j^g - \dot{u}^f \right) \right) \tag{11}$$

for a spatially constant bulk modulus of water K^f and volume fraction of water ϕ^f. The viscous friction coefficient is introduced as

$$\overline{\eta}_j = 4\pi n_j r_j \eta^{fR} = \frac{3\phi_j^g \eta^{fR}}{r_j^2}, \tag{12}$$

Equation (12) shows the distinct size effect of the gas-water mixture. Keeping the volume fraction of the gas phase ϕ_j^g constant and decreasing the radius of the gas bubbles the viscous behavior, i.e. the attenuation mechanism in the system, becomes more and more important (scales with $1/r_j^2$). This is obvious, as for smaller bubbles the ratio of surface to volume becomes bigger and bigger. Using Equations (7) and (12), Equation (11) can be further simplified:

$$\rho^f \ddot{u}^f = \phi^f K^f \frac{\partial^2 u^f}{\partial x^2} + \sum_{j=1}^{m}\left(\rho_j^g \omega_{0j}^2 \left(u_j^g - u^f\right)\right) + \sum_{j=1}^{m}\left(\overline{\eta}_j \left(\dot{u}_j^g - \dot{u}^f\right)\right). \tag{13}$$

2.3 Gas-water-mixture

For the mixture of water and gas, the momentum interaction terms must vanish (Equation (8)). Also, we assume that the bulk modulus of the gas-water-mixture is equal to the Reuss average (Mavko et al., 2003) of the bulk moduli of the two constituents, i.e. *Kg* for gas and *Kf* for water:

$$\frac{1}{K^{\text{Reuss}}} = \frac{\phi^g}{K^g} + \frac{\phi^f}{K^f}. \tag{14}$$

The Reuss average of the bulk moduli is plotted in Fig. 2 for the material parameters shown in Table 1 and for a range of gas volume fractions. Using Equation (14), the pressure of the gas-water-mixture can be expressed in terms of the deformation of the water phase while the deformation of the gas phase is taken into account through the Reuss average of the bulk moduli. Taking these considerations into account, the total momentum balance equation for the gas-water-mixture can be written as

$$\rho^f \ddot{u}^f + \sum_{j=1}^{m}\left(\rho_j^g \ddot{u}_j^g\right) = K^{\text{Reuss}} \frac{\partial^2 u^f}{\partial x^2}. \tag{15}$$

Subtracting Equation (13) from Equation (15) leads to the partial balance of momentum for the sum of the gas bubbles:

$$\sum_{j=1}^{m}\left(\rho_j^g \ddot{u}_j^g\right) = \left(K^{\text{Reuss}} - \phi^f K^f\right)\frac{\partial^2 u^f}{\partial x^2} - \sum_{j=1}^{m}\left(\rho_j^g \omega_{0j}^2 \left(u_j^g - u^f\right)\right) - \sum_{j=1}^{m}\left(\overline{\eta}_j \left(\dot{u}_j^g - \dot{u}^f\right)\right). \tag{16}$$

Equation (16) is split into *m* different equations, one for each bubble size in the system. The first term on the right-hand side is distributed among these *m* equations according to the relative volume fraction of gas inside a particular bubble size. The *m* equations are:

$$\rho_j^g \ddot{u}_j^g = \frac{\phi_j^g}{\phi^g}\left(K^{\text{Reuss}} - \phi^f K^f\right)\frac{\partial^2 u^f}{\partial x^2} - \rho_j^g \omega_{0j}^2 \left(u_j^g - u^f\right) - \overline{\eta}_j \left(\dot{u}_j^g - \dot{u}^f\right) \quad \text{for } j = \{1,\ldots,m\}. \tag{17}$$

2.2 Monochromatic acoustic wave

Next, we analyze monochromatic acoustic waves propagating through a medium that is described by the partial balance Equations (17) and (13). We apply a standard harmonic ansatz of the form

$$u^{\beta} = U^{\beta} \exp\left(i\left(kx - \omega t\right)\right) \tag{18}$$

with $\beta=\{g_1,...,g_m,f\}$ representing the individual phases. In Equation (18) U^{β} is the amplitude of the wave, i is the imaginary unit (i.e. i^2=-1), ω is angular frequency, t is time and k is the complex wave number. For the model containing bubbles with m different radii r_j with i={1,...,m} with the volume fractions ϕ_j^g we obtain

$$\begin{aligned}
&-\omega^2\rho_1^g U_1^g + \rho_1^g\omega_{01}^2\left(U_1^g - U^f\right) - i\omega\overline{\eta}_1\left(U_1^g - U^f\right) - \frac{\phi_1^g}{\phi^g}\left(\phi^f K^f - K^{\text{Reuss}}\right)k^2 U^f = 0,\\
&\qquad\qquad\vdots\\
&-\omega^2\rho_m^g U_m^g + \rho_m^g\omega_{0m}^2\left(U_m^g - U^f\right) - i\omega\overline{\eta}_m\left(U_m^g - U^f\right) - \frac{\phi_m^g}{\phi^g}\left(\phi^f K^f - K^{\text{Reuss}}\right)k^2 U^f = 0,\\
&\left(-\omega^2\rho^f + \phi^f K^f k^2 + \sum_{j=1}^{m}\left(\rho_j^g\omega_{0j}^2 - i\omega\overline{\eta}_j\right)\right)U^f - \sum_{j=1}^{m}\left(\rho_j^g\omega_{0j}^2 - i\omega\overline{\eta}_j\right)U_j^g = 0.
\end{aligned} \tag{19}$$

Equation (19) can be written in matrix notation as $(\mathbf{A}\text{-}k^2\mathbf{B})\mathbf{U}=0$, resulting in the generalized eigenvalue problem

$$\det\left(\mathbf{A} - k^2\mathbf{B}\right) = 0\,. \tag{20}$$

The vector $\mathbf{U}$ is defined as $\mathbf{U} = \begin{bmatrix} U_1^g & \dots & U_m^g & U^f \end{bmatrix}$ and the matrices $\mathbf{A}$ and $\mathbf{B}$ are given as

$$\mathbf{A} = \begin{bmatrix}
\left(\omega_{01}^2 - \omega^2\right)\rho_1^g - i\omega\overline{\eta}_1 & \dots & 0 & -\rho_1^g\omega_{01}^2 + i\omega\overline{\eta}_1\\
\vdots & \ddots & \vdots & \vdots\\
0 & \dots & \left(\omega_{0m}^2 - \omega^2\right)\rho_m^g - i\omega\overline{\eta}_m & -\rho_m^g\omega_{0m}^2 + i\omega\overline{\eta}_m\\
-\rho_1^g\omega_{01}^2 + i\omega\overline{\eta}_1 & \dots & -\rho_m^g\omega_{0m}^2 + i\omega\overline{\eta}_m & -\omega^2\rho^f + \sum_{j=1}^{m}\left(\rho_j^g\omega_{0j}^2 - i\omega\overline{\eta}_j\right)
\end{bmatrix}, \tag{21}$$

$$\mathbf{B} = \begin{bmatrix}
0 & \dots & 0 & \frac{\phi_1^g}{\phi^g}\left(\phi^f K^f - K^{\text{Reuss}}\right)\\
\vdots & \ddots & \vdots & \vdots\\
0 & \dots & 0 & \frac{\phi_m^g}{\phi^g}\left(\phi^f K^f - K^{\text{Reuss}}\right)\\
0 & \dots & 0 & -\phi^f K^f
\end{bmatrix}. \tag{22}$$

The solution of the generalized eigenvalue problem (Equation (20)) is the dispersion relation expressed by the frequency-dependent and complex wave number k, from which the phase velocity c and attenuation factor α of the acoustic wave can be calculated:

$$c = \frac{\omega}{\text{Re}\left(k\right)} \quad , \quad \alpha = \text{Im}\left(k\right). \tag{23}$$

In Equation (23), Re(k) and Im(k) denote the real and imaginary part of the complex wave number k, respectively.

3. Dispersion and frequency-dependent attenuation

The solution of the generalized eigenvalue problem (Equation (20)) is frequency-dependent and complex. Therefore, also the phase velocity c and the attenuation α is frequency-dependent. However, low and high frequency limits for the phase velocity can be determined:

$$\lim_{\omega\to 0}(c) = c^{\text{Wood}} = \sqrt{\frac{K^{\text{Reuss}}}{\rho^{\text{eff}}}} \quad , \quad \lim_{\omega\to\infty}(c) = c^{fR} = \sqrt{\frac{K^{\text{f}}}{\rho^{fR}}} \; . \tag{24}$$

The low-frequency-limit for the phase velocity is the so-called Wood-limit (Mavko et al., 2003). At frequencies much smaller than the resonance frequency of the gas bubbles, water and gas move in phase. Therefore, in this regime, effective material parameters have to be used, i.e. the Reuss average of the bulk moduli of the two constituents and the effective density of the gas-water-mixture, which is given as

$$\rho^{\text{eff}} = \rho^{f} + \rho^{g} = \rho^{f} + \sum_{j=1}^{m} \rho_j^g = \phi^f \rho^{fR} + \sum_{j=1}^{m} \left(\phi_j^g\right) \rho^{gR} = \phi^f \rho^{fR} + \phi^g \rho^{gR} \; . \tag{25}$$

The effective density and the Wood-limit is plotted in Fig. 2 together with the Reuss average of the bulk moduli (Equation (14)) for the material parameters shown in Table 1 and for a range of gas volume fractions. The high-frequency-limit for the phase velocity (Equation (24)) is equal to the phase velocity of bubble-free water c^{fR}. At frequencies much larger than the resonance frequency, inertia prohibits a movement of the gas bubbles. Therefore, in this regime, the true material parameters of the fluid have to be used.

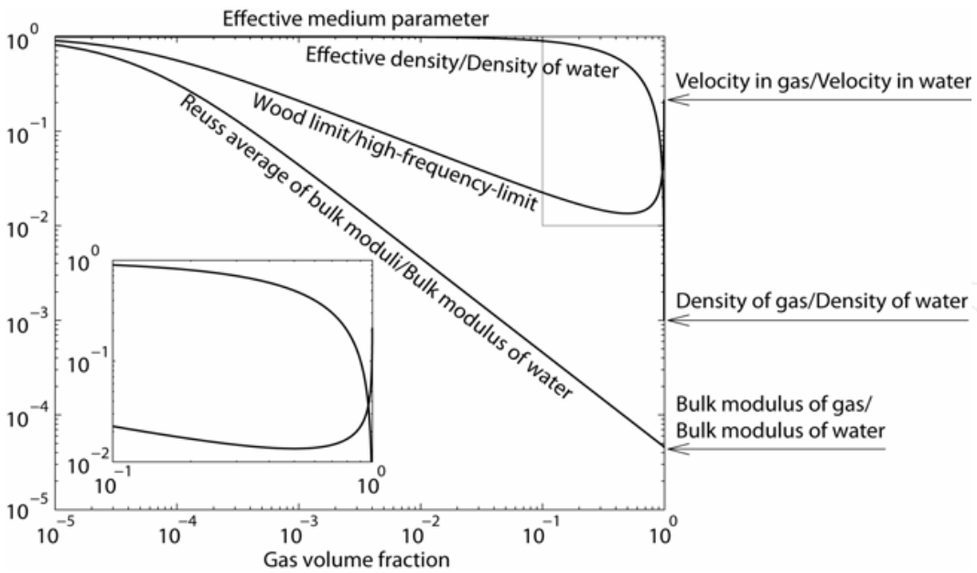

Fig. 2. Effective density ρ^{eff}, low-frequency-limit (i.e. Wood-limit) c^{Wood} and Reuss average of the bulk moduli K^{Reuss} for the material parameters shown in Table 1 and for a range of gas volume fractions. All values are dimensionless and normalization was done with the respective values for pure water, i.e. the high-frequency-limits. The gray box in the upper right corner is blown up and shown as the inlet in the lower left of the figure.

	Parameter	Symbol	Value [Unit]
Water	Density	ρ^{fR}	1000 [kg/m^3]
	Bulk modulus	K^f	2.2x10^9 [Pa]
	Viscosity	η^{fR}	1x10^{-3} [Pa s]
	Sound speed	c^{fR}	1483 [m/s]
Gas	Density	ρ^{gR}	1 [kg/m^3]
	Bulk modulus	K^g	101x10^3 [Pa]
	Heat capacity ratio	γ	1.4 [-]
	Sound speed	c^{gR}	362 [m/s]
Water depth		H	0 [m]

Table 1. Physical properties of the pure media used in this study, i.e. bubble-free water and pure gas, respectively, and the water depth that is common to all models in this study.

We define the resonance frequency ω_{0j} of our coupled wave propagation-oscillator model to be the frequency where the peak attenuation occurs. The resonance frequency is

$$\omega_{0j} = A\Omega_{0j} = \frac{c^{fR}}{c^{Wood}}\Omega_{0j} \,. \tag{26}$$

Equation (26) shows that the scaling factor A is not an arbitrary value, but is a combination of material parameters defined earlier, i.e. the ratio between high- and low-frequency-limit of the phase velocity.

3.1 Gas bubbles of only one size

First, we study a model containing gas bubbles of only one size. Consequently, only the first and the last equations of the set of Equations (19) are used and matrices **A** and **B** (Equations (21) and (22)) reduce to 2x2-matrices. Fig. 3 and Fig. 4 both show the phase velocity dispersion (a) and the frequency-dependent attenuation (b) of acoustic waves in such a model. The material parameters used for producing Fig. 3 and Fig. 4 are given in Table 1. In Fig. 3 the gas volume fraction is constant (ϕ^g=0.001) for all lines while the different lines represent different gas bubble sizes (r={7x10^{-5}m, 1x10^{-4}m, 2x10^{-4}m, 5x10^{-4}m, 1x10^{-3}m}). These gas bubble sizes result in angular resonance frequencies Ω_0={2.93x10^{5}Hz, 2.05x10^{5}Hz, 1.02x10^{5}Hz, 4.10x10^{4}Hz, 2.05x10^{4}Hz}. In Fig. 4 the gas bubble size is constant (r=2x10^{-4}m, ω_0=1.02x10^{5}Hz) for all lines while the different lines represent different gas volume fractions (ϕ^g={1x10^{-4}, 5x10^{-4}, 1x10^{-3}, 5x10^{-3}, 1x10^{-2}}).

For a constant gas volume fraction the low- and high-frequency-limit for the phase velocity (Fig. 3a) is also constant. This is obvious because these limits (Equations (24)) only depend on the effective material properties of the gas-water-mixture (i.e. Reuss average of bulk moduli and effective density) and on the material properties of water, respectively, and not on the size of the gas bubbles. However, the size of the gas bubbles influences the phase velocity dispersion curves in the vicinity of the resonance frequency of the gas bubbles. For small gas bubbles, the attenuation becomes more important (Equation (12)) and the oscillations are damped more. Therefore, not such a strong excitation of the oscillations can take place and the transition from the low- to the high-frequency-limit of the phase velocity dispersion curve is smoother for small gas bubble sizes, i.e. not such strong minimum and maximum values. On the other hand, for larger bubble sizes, the damping is small and the

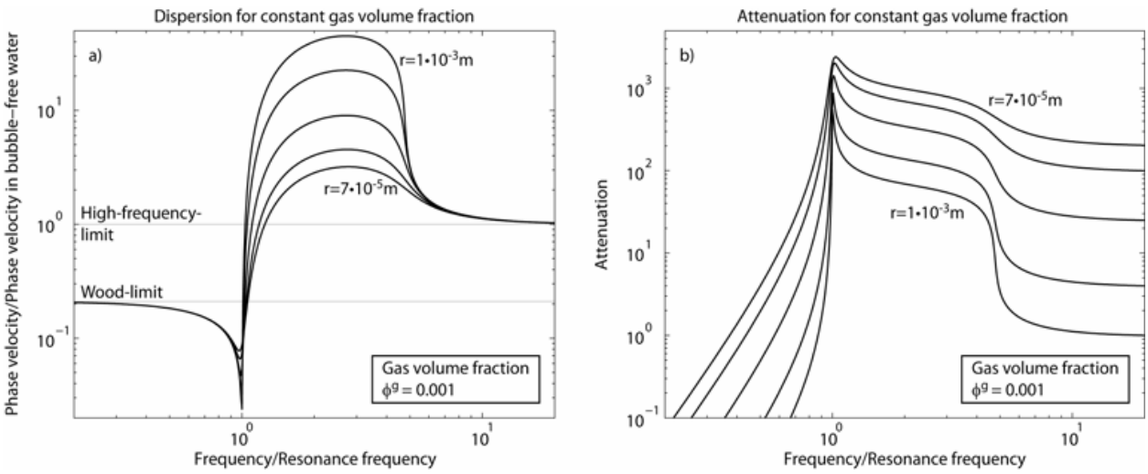

Fig. 3. Dispersion (a) and frequency-dependent attenuation (b) for water containing gas with a fixed volume fraction ϕg=0.001. Material parameters are given in Table 1. While the gas volume fraction is kept constant, for each curve the gas volume is contained in bubbles with equal radius (in meter) r={7x10^{-5}, 1x10^{-4}, 2x10^{-4}, 5x10^{-4}, 1x10^{-3}}. The frequency is normalized with the resonance frequency and the phase velocity is normalized with the phase velocity in bubble-free water, i.e. with the high-frequency-limit.

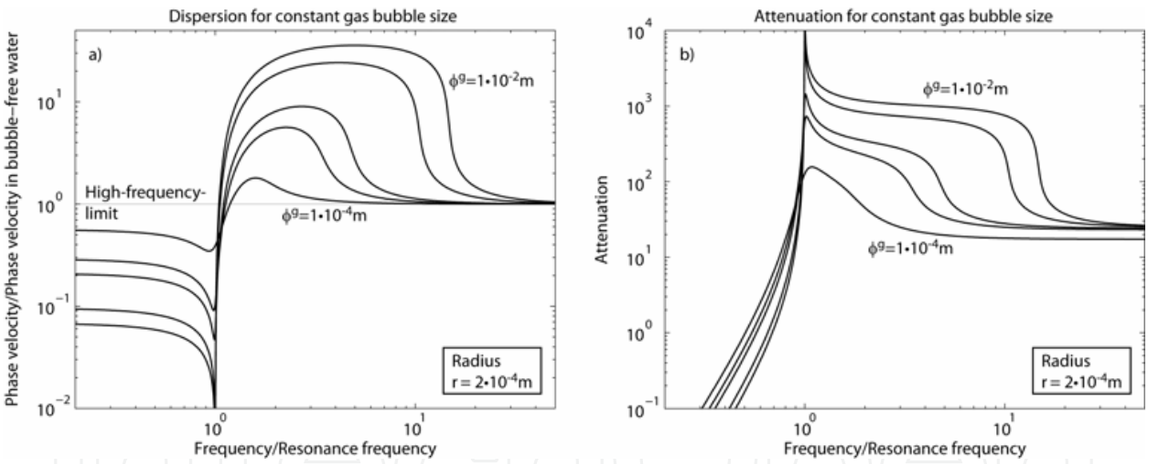

Fig. 4. Dispersion (a) and frequency-dependent attenuation (b) for water containing gas bubbles with a fixed radius r=2x10^{-4}m. Material parameters are given in Table 1. While the gas bubble size is kept constant, the gas volume fraction is different for the different lines (ϕg={1x10^{-4}, 5x10^{-4}, 1x10^{-3}, 5x10^{-3}, 1x10^{-2}}). The frequency is normalized with the resonance frequency and the phase velocity is normalized with the phase velocity in bubble-free water, i.e. with the high-frequency-limit.

oscillations are strongly excited. For all bubble sizes, at frequencies slightly lower than the resonance frequency, the phase velocity strongly decreases before it rapidly increases to values much larger than the high-frequency-limit. For increasing frequencies, the phase velocity decreases to eventually reach the high-frequency-limit. Such a behavior of the phase velocity around the resonance frequency was also described by van Wijngaarden (1972), Anderson and Hampton (1980) or Commander and Prosperetti (1989).

The effect of the gas bubble size on attenuation is shown in Fig. 3b. Around the resonance frequency, the attenuation of an acoustic wave is largest because energy is transferred from the water to the gas bubbles to excite the oscillations. At frequencies much larger than the resonance frequency, inertia prohibits a movement of the gas bubbles. Obviously, the non-moving gas bubbles damp a propagating acoustic wave. As described above, the attenuation depends on the gas bubble size (Equation (12)). At frequencies much smaller than the resonance frequency of the gas bubbles, water and gas move in phase. Therefore, there is no relative movement between gas and water and consequently no attenuation.
The phase velocity dispersion curves for different gas volume fractions but for constant gas bubble size (Fig. 4a) are qualitatively comparable. The major difference between these curves is the low-frequency-limit. A smaller gas volume fraction leads to a larger value of the Reuss average of the bulk moduli (Equation (14)) and therefore to a higher value of the low-frequency-limit of the phase velocity (Equation (24)). At the same time, the influence on the Wood-limit of the change of the effective density (Equation (25)) with changing gas volume fraction is only minimal in the range considered in Fig. 4. This can also be observed in Fig. 2. The attenuation of an acoustic wave (Fig. 4b) is stronger for larger gas volume fractions. This is intuitive, because the larger the gas volume fraction is, the more gas bubbles are present in the water and the stronger water and gas interact. However, the high-frequency-limit for the attenuation is only weakly influenced by the gas volume fraction with a slightly higher attenuation for larger gas volume fractions. From the equation for viscous friction term $\overline{\eta}$ (Equation (12)) it is clear that the bubble radius (Fig. 3b) has a much stronger influence on the attenuation than the gas volume fraction (Fig. 4b), i.e. quadratic vs. linear relation, respectively.

3.2 Gas bubbles with two different sizes

The model equation (Equations (13) and (17)) are written for an arbitrary number of gas bubble sizes. Exemplarily, we consider two different bubble sizes in the water, leading to two different resonance frequencies. The material parameters for gas and water are given in Table 1 and the two bubble sizes and volume fractions are given in Table 2. The volume fraction of the total number of bubbles of each bubble size is equal, i.e. half of the gas is contained in one bubble size, the other half is contained in the other bubble size. Fig. 5 shows the phase velocity dispersion (a) and frequency-dependent attenuation (b) for this model. The low- and high-frequency-limits for the phase velocity are the same as in Fig. 3, because the gas volume fraction is the same. However, the dispersion curve in the vicinity of the two resonance frequencies is quite different. The typical dispersion behavior for only one bubble size shown in Fig. 3 and Fig. 4 (i.e. decreasing velocity below resonance frequency, rapid increase to values larger than high-frequency-limit, decrease to high-frequency-limit) takes place twice, once at each of the two resonance frequencies. Therefore, two, rather than one, sets of minimum and maximum occur in the phase velocity dispersion curve (Fig. 5a). For comparison, the dispersion and the frequency-dependent attenuation of two models containing only either of the two bubble sizes with their respective volume fraction are also plotted in Fig. 5. Note that the scaling of the resonance frequencies is different for these models because the total gas volume fraction is different. As for the phase velocity dispersion, the attenuation (Fig. 5b) shows two maxima, one at each of the two resonance frequencies.

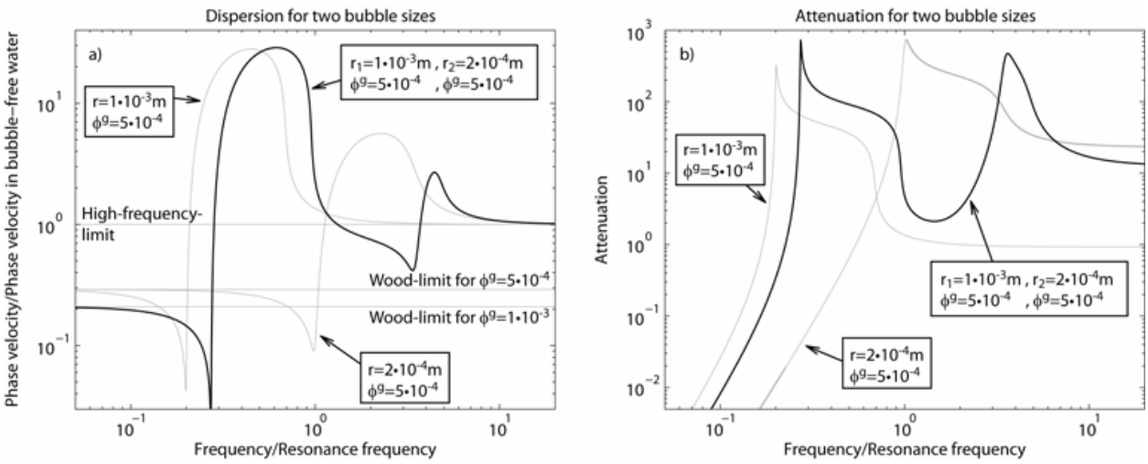

Fig. 5. Dispersion (a) and frequency-dependent attenuation (b) for water containing gas bubbles with two different radii r_1=1x10^{-3}m and r_2=2x10^{-4}m. Material parameters are given in Table 1 and Table 2. Plotted in light gray for comparison are the dispersion and the frequency-dependent attenuation of two models containing only either of the two bubble sizes with their respective volume fraction. The frequency is normalized with the resonance frequency of the larger bubble and the phase velocity is normalized with the phase velocity in bubble-free water, i.e. with the high-frequency-limit.

Parameter	**Value [Unit]**	
Gas volume fraction	ϕ^g=1x10^{-3} [-]	
	Gas bubble size 1	**Gas bubble size 2**
Bubble radius	r_1=1x10^{-3} [m]	r_2=2x10^{-4} [m]
Volume fraction of gas bubble sizes	ϕ_1^g =5x10^{-4} [-]	ϕ_2^g =5x10^{-4} [-]
Angular resonance frequency	ω_{01}=2.05x10^4 [Hz]	ω_{02}=1.02x10^5 [Hz]

Table 2. Model parameters for the model containing gas bubbles of two different sizes. Material parameters for gas and water are given in Table 1.

3.3 Probability function for gas bubble sizes

The model equation (Equations (13) and (17)) are written for an arbitrary number of gas bubble sizes. In principle, every gas bubble size distribution can be approximated by a combination of discrete size (i.e. radius) and volume fraction distributions, which can then be used in Equations (13) and (17). Exemplarily, we show results for bubble radii that lie in the range [0.1r_0...10r_0] and whose corresponding volume fractions are log-normal distributed around a central value r_0. The following equation describes the distribution of the volume fraction for the different bubble sizes:

$$\phi_j^g = \Phi \exp\left(\frac{-\left(\ln\left(r_j\right) - \ln\left(r_0\right)\right)^2}{s^2} \right) \quad \text{for } r_j \in \left[0.1r_0 \ldots 10r_0\right] \text{ and } j = \left\{1,\ldots,501\right\}. \tag{27}$$

We set r_0=2x10^{-4}m and we pick 501 values for the bubble radius r_j in the range [0.1r_0...10r_0] in a way that the logarithm of r_j is equally spaced. The factor Φ is chosen in such a way that

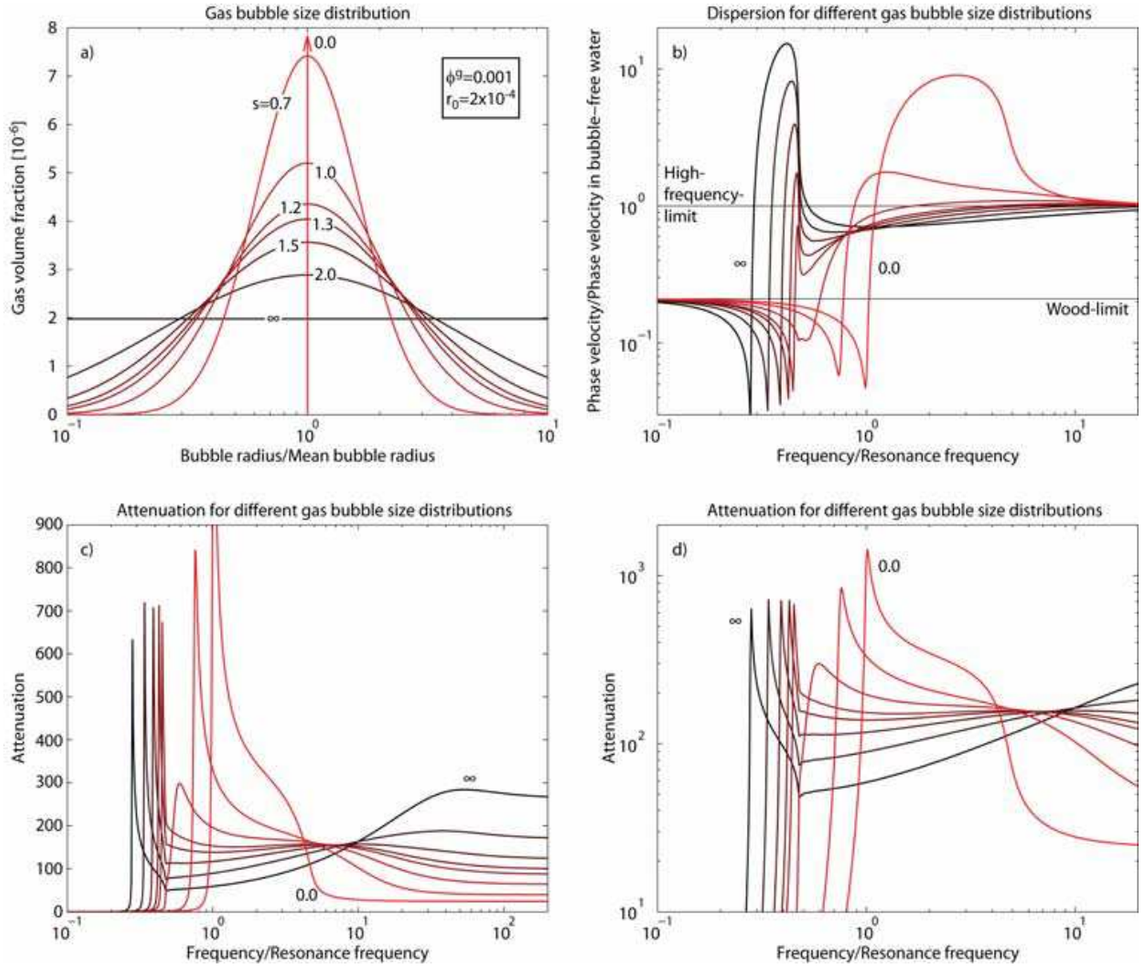

Fig. 6. a) Gas volume fraction versus bubble radius. The bubble radius is normalized with r_0=2x10^{-4}m. Along these curves, 501 discrete values are picked at equally spaced values for the logarithm of the bubble radius, i.e. the curves are discrete probability functions, rather than continuous ones. The sum of all 501 values is equal to ϕ^g=0.001. Labels correspond to the values of parameter s in Equation (27). The curve with label "0.0" corresponds to a model with only one bubble size. b), c) and d) Dispersion and two different representations of the frequency-dependent attenuation for water containing gas with a fixed volume fraction ϕ^g=0.001 and with bubble size distributions shown in a). Labels are only given for the end member curves. All other curves correspond to the curves labeled in a). Material parameters are given in Table 1. The frequency is normalized with the resonance frequency and the phase velocity is normalized with the phase velocity in bubble-free water, i.e. with the high-frequency-limit.

Equations (6) are fulfilled for a gas volume fraction ϕ^g=0.001. Equation (27) describes the discrete approximation of a log-normal probability function. The log-normal function is cut off at the values $0.1r_0$ and $10r_0$ because bubble radii only lie between these two values. In Fig. 6a, Equation (27) is plotted for different values of the parameter s (i.e. s={0.0, 0.7, 1.0, 1.2, 1.3, 1.5, 2.0, ∞}). Choosing s=∞ (infinity) results in a flat distribution where the volume fraction for each bubble size is equal. Choosing s=0 results in a Dirac-distribution where

only one bubble size is present, i.e. bubbles with radius r_0. In Fig. 6 the phase velocity dispersion (b) and the frequency-dependent attenuation (c and d) are shown for the different distribution functions shown in Fig. 6a. Note that curves labeled "0.0" correspond to a model with only one bubble size and are the same as the third curves in Fig. 3 and Fig. 4.
The high- and low-frequency-limits for the phase velocity is equal for all bubble size distributions because the gas volume fraction ϕ_g is equal. Between the two limits, the different bubble size distributions lead to significantly different dispersion curves. Only the first and second curve (i.e. s={0.0, 0.7}), for which only one gas bubble size occurs or the gas bubble size is very narrowly distributed around r_0, respectively, show the characteristic features described above for Fig. 3a and Fig. 4a (i.e. maximum peak velocity and asymptotic approach of the high-frequency-limit). For wider gas bubble size distributions, the clear maximum peak disappears and the asymptotic approach of the high-frequency-limit is very flat or even from values smaller than the high-frequency-limit. For larger values of s (i.e. s={1.3, 1.5, 2.0, ∞}), the phase velocity exhibits a maximum value that is higher than the high-frequency-limit and drops below the high-frequency-limit for increasing frequencies.
The attenuation shows different characteristics in the high-frequency-range (Fig. 6c) and at frequencies around the central resonance frequency (Fig. 6d). The high-frequency-limit strongly resembles the behavior described for Fig. 3b, where models containing equally sized gas bubbles were analyzed for different bubble sizes. A wider gas bubble size distribution (larger value for parameter s) introduces more small gas bubbles compared to large ones. The small gas bubbles dominate the attenuation characteristics in the high-frequency-limit. In the vicinity of the central resonance frequency the attenuation curves show a distinct peak. This peak changes its maximum value with changing bubble size distribution. It is roughly constant for large values of s (i.e. s={1.2, 1.3, 1.5, 2.0, ∞}), has a minimum for s=1.0 and becomes larger for small values of s (i.e. s={0.0, 0.7}).

3.4 Comparison with existing models

We compare our phase velocity dispersion and attenuation curves with existing and published curves. First, we consider two curves of Commander and Prosperetti (1989). Figures 1 and 8 of Commander and Prosperetti (1989) show the dispersion and phase velocity, respectively, of water containing gas bubbles with only one size (r=9.94x10^{-4}m) and a gas volume fraction ϕ_g=3.77x10^{-4}. Also, it is shown that the theory of Commander and Prosperetti (1989) matches the experimental data of Silberman (1957) for the same model conditions. Fig. 7 compares the two figures of Commander and Prosperetti (1989) with our model for the same model parameters. The phase velocity dispersion matches the model of Commander and Prosperetti (1989) very well. All, the low-frequency-limit, the high-frequency-limits and the complicated dispersion behavior in the vicinity of the resonance frequency is almost identical. Also, the data of Silberman (1957) is equally well matched by our model in comparison with the model of Commander and Prosperetti (1989). Attenuation in Commander and Prosperetti (1989) is given in dB/cm, that is, a logarithmic unit with an arbitrary reference value. Therefore, we also plot the attenuation in logarithmic units and move the curve of Commander and Prosperetti (1989) vertically to adjust the two curves to the same reference value. Doing this does not change the vertical scale of either of the curves. It only changes the absolute values on the vertical axis. Our model matches the

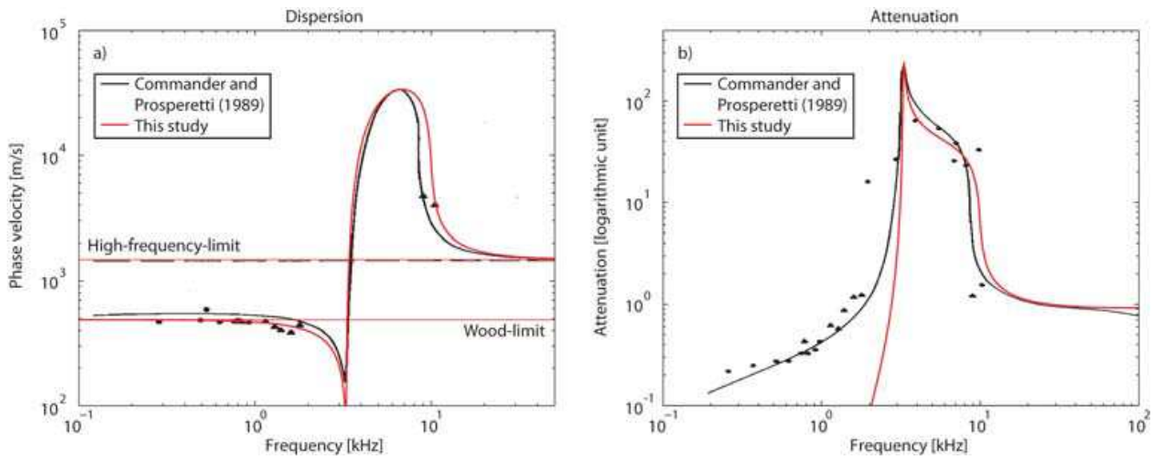

Fig. 7. Phase velocity dispersion (a) and frequency-dependent attenuation (b) for a model with one gas bubble size r=9.94x10^{-4}m and a gas volume fraction ϕ=3.77x10^{-4}. Plotted in black are Figures 8 and 1 of Commander and Prosperetti (1989). Data points are also taken from Commander and Prosperetti (1989), who took the data from Silberman (1957). All values are plotted as absolute values. In b), attenuation is plotted as a logarithmic unit, because in Commander and Prosperetti (1989) the attenuation is given in dB/cm.

model of Commander and Prosperetti (1989) very well in the frequency range at and above the resonance frequency. Here, also the attenuation data of Silberman (1957) is matched equally well in comparison with the model of Commander and Prosperetti (1989). However, in the frequency range below the resonance frequency the two models diverge from each other. The model of Commander and Prosperetti (1989) matches the data of Silberman (1957) significantly better compared to our model.

The second model we chose is the model by MacPherson (1957). Because no phase velocity dispersion curve is plotted in MacPherson (1957), we take Figure 10 of Anderson and Hampton (1980) who plot the phase velocity dispersion of MacPherson (1957). The model describes acoustic waves in water containing gas bubbles of one size. Fig. 8 compares Figure 10 of Anderson and Hampton (1980) with our model. In Anderson and Hampton (1980) it is unclear which bubble size is used for Figure 10. Therefore, we plot the two extreme values described by MacPherson (1957) (i.e. r=8x10^{-5}m and r=2.5x10^{-4}m) to have the possible range of bubble sizes. Also, in Figure 10 of Anderson and Hampton (1980) a gas volume fraction ϕ=1x10^{-3} is indicated. However, the Wood-limit (i.e. low-frequency-limit) is matched for a gas volume fraction ϕ=7x10^{-4}. We assume that the value given by Anderson and Hampton (1980) is only an approximation and we chose ϕ=7x10^{-4} for Fig. 8. The general trend of the phase velocity dispersion curve of Anderson and Hampton (1980) is well matched by our model, especially in the frequency range at and below the resonance frequency, where our model almost perfectly matches the curve of Anderson and Hampton (1980). However, in the frequency range above the resonance frequency, the two models diverge from each other.

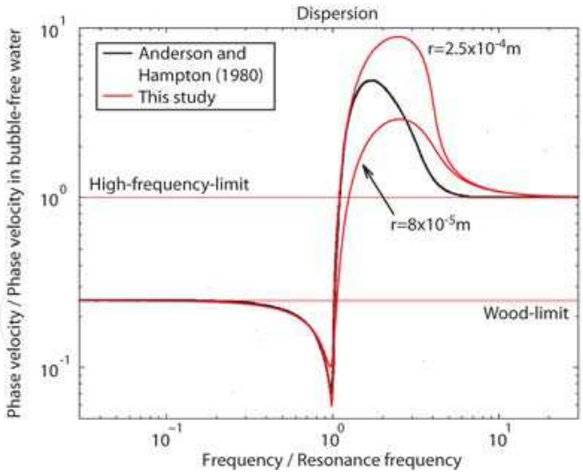

Fig. 8. Phase velocity dispersion for a model with one bubble size and a gas volume fraction ϕ_g=7x10^{-4}. Plotted in red are two dispersion curves for two different bubble radii r=8x10^{-5}m and r=2.5x10^{-4}m. Plotted in black is Figure 10 of Anderson and Hampton (1980). The frequency is normalized with the resonance frequency and the phase velocity is normalized with the phase velocity in bubble-free water, i.e. with the high-frequency-limit.

4. Discussion

There are many features that can generate oscillations and resonances in a medium through which acoustic and seismic waves propagate. Examples are air bubbles in water, holes in elastic plates, oil blobs in porous rocks or fluid-filled fractures in rocks. All oscillation processes exhibit a resonance frequency and the propagation of waves having frequencies in the range of about one order of magnitude around the resonance frequency will be considerably affected by these oscillations. The internal oscillations cause a dispersion and a frequency-dependent attenuation of the waves and consequently cause a frequency-dependent reflection and transmission behaviour of the medium exhibiting oscillations. Equations describing the coupling of wave propagation and oscillations are important, first, to better understand the general impact of oscillations on the wave propagation and, second, to apply these equations in inversion problems which aim to determine the size and distribution of heterogeneities causing oscillations inside a medium by analysing the waves that propagated through this medium. However, an exact mathematical treatment of the coupling between wave propagation and resonant oscillations is not trivial. For example, the propagation of acoustic waves in water with air bubbles may appear at first as a relatively simple process, but the process is actually quite complex and the exact mathematical treatment is complicated (e.g. Caflisch et al., 1985). An exact mathematical treatment of even more complicated processes, such as for example the wave propagation in partially saturated poroelastic solids with isolated fluid blobs, may be too complicated to be of practical use. Therefore, there is a need for a simple, more basic, mathematical description of wave propagation in media exhibiting oscillations.

We present here one basic mathematical approach to couple macroscopic wave propagation with microscopic oscillations. We assume that the oscillations (whatever the exact physical mechanism) can be effectively described with the equation for a damped linear oscillator.

We then couple the oscillator equation to the wave equation using the mixture theory. The coupling of the microscopic oscillations with the macroscopic wave propagation is done through moment interaction terms. We consider two interaction terms where one term scales with the volume and represents inertial coupling and the other term scales with the surface and represents the viscous coupling. With this approach it is easy to "switch" the coupling terms on and off and investigate their impact on the dispersion and attenuation. For example, Frehner et al. (2009) studied the coupling through only inertial terms and observed in a narrow frequency range around the resonance frequency a significant dispersion with a discontinuity of the phase velocity at the resonance frequency.
For acoustic waves propagating through water with air bubbles the dispersion and attenuation curves resulting from our approach agree well with the corresponding dispersion and attenuation curves resulting from more elaborated mathematical theories and also from laboratory experiments. This indicates that our approach captures the essential first-order effects of wave propagation in a medium with oscillations. Our approach also allows an easy extension to an arbitrary number of oscillators providing a particular distribution of resonance frequencies. Clearly, an exact mathematical treatment is always helpful and important to, for example, provide the range of applicability for the simplified equations.
Our approach can be applied to more complicated processes and we expect it to also capture the first-order effects on dispersion and attenuation. The equations resulting from our approach are more transparent and easier to use for inversion problems. Inversions are of great industrial and scientific interest because they allow to assess the distribution and amount of heterogeneities inside a medium by analyzing waves that propagated through the medium. An example is the determination of the bubble distribution in sea water near the ocean surface (e.g. Commander and McDonald, 1991).

5. Conclusions

Oscillations with a certain resonance frequency within a medium is a common physical phenomenon that takes place in a large number of media, e.g. porous or fractured rocks, water containing gas bubbles or heterogeneous media in general. Internal oscillations lead to a strongly frequency-dependent propagation behavior of waves that propagate through such media, i.e. velocity dispersion and frequency-dependent attenuation. However, such oscillations are usually not included in effective medium theories for heterogeneous media. We presented a one-dimensional continuum model for an acoustic medium exhibiting internal damped oscillations. It is a two- (or more) phase model with one connected elastic (i.e. acoustic) phase and one (or more) disconnected oscillating phase. The obvious application of this model is water containing oscillating gas bubbles. This application provided the material and model parameters used in this study. However, the material and model parameters could be adapted to other applications of a medium exhibiting internal oscillations. The presented model of water containing gas bubbles includes two physically based momentum interaction terms between the two phases, a purely elastic term of oscillatory nature that scales with the volume of the bubbles and a viscous term that scales with the specific surface of the bubble. Thus we are able to take into account damping with respect to the specific surface area of the gas bubbles. The model is capable of taking into

account a large number of oscillators with different resonance frequencies. In the limit case, a continuous probability function for the resonance frequencies can be approximated with a discrete number of oscillators. Exemplarily, we showed volume fractions that are log-normally distributed with respect to bubble size. The results show that a certain distribution of resonance frequencies around a central value changes the phase velocity dispersion and frequency-dependent attenuation significantly compared to the case where only one bubble size is present. The dispersion and attenuation resulting from our approach agree well with the dispersion and attenuation (1) derived with a more exact mathematical treatment and (2) measured in laboratory experiments. Hence, our basic approach captures the first-order effects of oscillations on the propagation of acoustic waves.

6. References

Aki, K. & Richards, P. G. (2002). *Quantitative seismology*, University Science Books, ISBN 0-9357-0296-2, Sausalito

Anderson, A. L. & Hampton, L. D. (1980). Acoustics of gas-bearing sediments, 1. Background. *Journal of the Acoustical Society of America*, 67, 6, 1865-1889, ISSN 0001-4966

Batchelor, G. K. (2000). *An introduction to fluid dynamics*. Cambridge University Press, ISBN 0-2516-6396-2, Cambridge

Beresnev, I. A. & Johnson, P. A. (1994). Elastic-wave stimulation of oil production - A review of methods and results. *Geophysics*, 59, 6, 1000-1017, ISSN 0016-8033

Beresnev, I. A., Vigil, R. D., Li, W. Q., Pennington, W. D., Turpening, R. M., Iassonov, P. P. & Ewing, R. P. (2005). Elastic waves push organic fluids from reservoir rock. *Geophysical Research Letters*, 32, 13, L13303, ISSN 0094-8276

Biot, M. A. (1962). Mechanics of deformation and acoustic propagation in porous media. *Journal of Applied Physics*, 33, 4, 1482-1498, ISSN 0021-8979

Bowen, R. M. (1980). Incompressible porous media models by use of the theory of mixtures. *International Journal of Engineering Science*, 18, 9, 1129–1148, ISSN 0020-7225

Bowen, R. M. (1982). Compressible porous media models by use of the theory of mixtures. *International Journal of Engineering Science*, 20, 6, 697–735, ISSN 0020-7225

Caflisch, R. E., Miksis, M. J., Papanicolaou, G. C. & Ting, L. (1985). Effective equations for wave propagation in bubbly liquids. *Journal of Fluid Mechanics*, 153, April, 259-273, ISSN 0022-1120

Carstensen, E. L. & Foldy, L. L. (1947). Propagation of sound through a liquid containing bubbles. *Journal of the Acoustical Society of America*, 19, 3, 481-501, ISSN 0001-4966

Commander, K. W. & McDonald, R. J. (1991). Finite-element solution of the inverse problem in bubble swarm acoustics. *Journal of the Acoustical Society of America*, 89, 2, 592-597, ISSN 0001-4966

Commander, K. W. & Prosperetti, A. (1989). Linear pressure waves in bubbly liquids: Comparison between theory and experiments. *Journal of the Acoustical Society of America*, 85, 2, 732-746, ISSN 0001-4966

Dutta, N. C. & Ode, H. (1979). Attenuation and dispersion of compressional waves in fluid-filled porous rocks with partial gas saturation (White model). 1. Biot theory. *Geophysics*, 44, 11, 1777-1788, ISSN 0016-8033

Dvorkin, J., Mavko, G. & Nur, A. (1990). The oscillations of a viscous compressible fluid in an arbitrarily-shaped pore. *Mechanics of Materials*, 9, 2, 165-179, ISSN 0167-6636

Fox, F. E., Curley, S. R. & Larson, G. S. (1955). Phase velocity and absorption measurements in water containing air bubbles. *Journal of the Acoustical Society of America*, 27, 3, 534-539, ISSN 0001-4966

Frehner, M., Schmalholz, S. M. & Podladchikov, Y. (2009). Spectral modification of seismic waves propagating through solids exhibiting a resonance frequency: A 1-D coupled wave propagation–oscillation model. *Geophysical Journal International*, 176, 2, 589-600, ISSN 0956-540X

Frehner, M., Schmalholz, S. M., Saenger, E. H. & Steeb, H. (2008). Comparison of finite difference and finite element methods for simulating two-dimensional scattering of elastic waves. *Physics of the Earth and Planetary Interiors*, 171, 1-4, 112-121, ISSN 0031-9201

Graham, D. R. & Higdon, J. J. L. (2000). Oscillatory flow of droplets in capillary tubes. Part 1 and 2. *Journal of Fluid Mechanics*, 425, 31-53 and 55-77, ISSN 0022-1120

Hassan, W. & Nagy, P. B. (1997). Circumferential creeping waves around a fluid-filled cylindrical cavity in an elastic medium. *Journal of the Acoustical Society of America*, 101, 5, 2496-2503, ISSN 0001-4966

Hilpert, M. (2007). Capillarity-induced resonance of blobs in porous media: Analytical solutions, Lattice-Boltzmann modeling, and blob mobilization. *Journal of Colloid and Interface Science*, 309, 2, 493-504, ISSN 0021-9797

Hilpert, M., Jirka, G. H. & Plate, E. J. (2000). Capillarity-induced resonance of oil blobs in capillary tubes and porous media. *Geophysics*, 65, 3, 874-883, ISSN 0016-8033

Iassonov, P. P. & Beresnev, I. A. (2003). A model for enhanced fluid percolation in porous media by application of low-frequency elastic waves. *Journal of Geophysical Research B: Solid Earth*, 108, 3, ESE 2-1-ESE 2-9, ISSN 0148-0227

Kelly, K. R. & Marfurt, K. J. (1990). *Numerical Modeling of Seismic Wave Propagation*. Society of Exploration Geophysicists, ISBN 1-56080-011-9, Tulsa, Oklahoma

Korneev, V. (2008). Slow waves in fractures filled with viscous fluid. *Geophysics*, 73, 1, N1-N7, ISSN 0016-8033

Korneev, V. (2009). Resonant seismic emission of subsurface objects. *Geophysics*, 74, 2, T47-T53, ISSN 0016-8033

Korneev, V. A., Goloshubin, G. M., Daley, T. M. & Silin, D. B. (2004). Seismic low-frequency effects in monitoring fluid-saturated reservoirs. *Geophysics*, 69, 2, 522-532, ISSN 0016-8033

Lee, S.-L., Komatitsch, D., Huang, B.-S. & Tromp, J. (2009). Effects of topography on seismic-wave propagation: An example from northern Taiwan. *Bulletin of the Seismological Society of America*, 99, 1, 314-325, ISSN 0037-1106

Li, W. Q., Vigil, R. D., Beresnev, I. A., Iassonov, P. & Ewing, R. (2005). Vibration-induced mobilization of trapped oil ganglia in porous media: Experimental validation of a capillary-physics mechanism. *Journal of Colloid and Interface Science*, 289, 1, 193-199, ISSN 0021-9797

Liu, Y. B., Wu, R. S. & Ying, C. F. (2000). Scattering of elastic waves by an elastic or viscoelastic cylinder. *Geophysical Journal International*, 142, 2, 439-460, ISSN 0956-540X

MacPherson, J. D. (1957). The effect of gas bubbles on sound propagation in water. *Proceedings of the Physical Society. Section B*, 70, 1, 85-92, ISSN 0370-1301

Martin, R. & Komatitsch, D. (2009). An unsplit convolutional perfectly matched layer technique improved at grazing incidence for the viscoelastic wave equation. *Geophysical Journal International*, 179, 1, 333-344, ISSN 0956-540X

Mavko, G., Mukerji, T. & Dvorkin, J. (2003). *The rock physics handbook: Tools for seismic analysis in porous media*. Cambridge University Press, ISBN 0-5215-4344-4, Cambridge

Minnaert, M. (1933). On musical air bubbles and the sound of running water. *Philosophical Magazine*, 16, 104, 235-248, ISSN 1478-6435

Pride, S. R., Flekkoy, E. G. & Aursjo, O. (2008). Seismic stimulation for enhanced oil recovery. *Geophysics*, 73, 5, O23-O35, ISSN 0016-8033

Quintal, B., Schmalholz, S. M. & Podladchikov, Y. Y. (2009). Low-frequency reflections from a thin layer with high attenuation caused by interlayer flow. *Geophysics*, 74, 1, N15-N23, ISSN 0016-8033

Saenger, E. H., Ciz, R., Krüger, O. S., Schmalholz, S. M., Gurevich, B. & Shapiro, S. A. (2007). Finite-difference modeling of wave propagation on microscale: A snapshot of the work in progress. *Geophysics*, 72, 5, SM293-SM300, ISSN 0016-8033

Santos, J. E., Douglas, J., Corbero, J. & Lovera, O. M. (1990). A model for wave-propagation in a porous-medium saturated by a 2-phase fluid. *Journal of the Acoustical Society of America*, 87, 4, 1439-1448, ISSN 0001-4966

Schultz, T., Cattafesta, L. N. & Sheplak, M. (2006). Modal decomposition method for acoustic impedance testing in square ducts. *Journal of the Acoustical Society of America*, 120, 6, 3750-3758, ISSN 0001-4966

Silberman, E. (1957). Sound velocity and attenuation in bubbly mixtures measured in standing wave tubes. *Journal of the Acoustical Society of America*, 29, 8, 925-933, ISSN 0001-4966

Smeulders, D. M. J. & van Dongen, M. E. H. (1997). Wave propagation in porous media containing a dilute gas-liquid mixture: Theory and experiments. *Journal of Fluid Mechanics*, 343, 351-373, ISSN 0022-1120

Truesdell, C. A. (1957). Sulle basi della termomeccanica I & II, *Accademia Nazionale dei Lincei, Rendiconti della Classe di Scienze Fisiche, Matematiche e Naturali*, 8, 22, 33-38 and 158-166

Urquizu, M. & Correig, A. M. (2004). On the equivalence between stratified media and oscillators. *Geophysical Journal International*, 157, 1, 245-250, ISSN 0956-540X

van Wijngaarden, L. (1972). One-dimensional flow of liquids containing small gas bubbles. *Annual Review of Fluid Mechanics*, 4, 369-396, ISSN 0066-4189

Wei, C. F. & Muraleetharan, K. K. (2002). A continuum theory of porous media saturated by multiple immiscible fluids: I. Linear poroelasticity. *International Journal of Engineering Science*, 40, 16, 1807-1833, ISSN 0020-7225

Werby, M. F. & Gaunaurd, G. C. (1990). Resonance scattering from submerged elastic spheroids of high aspect ratios and its 3-dimensional interpretation. *Journal of the Acoustical Society of America*, 88, 2, 951-960, ISSN 0001-4966

White, J. E. (1975). Computed seismic speeds and attenuation in rocks with partial gas saturation. *Geophysics*, 40, 2, 224-232, ISSN 0016-8033

Wave Propagation in Materials for Modern Applications

Edited by Andrey Petrin

ISBN 978-953-7619-65-7
Hard cover, 526 pages
Publisher InTech
Published online 01, January, 2010
Published in print edition January, 2010

In the recent decades, there has been a growing interest in micro- and nanotechnology. The advances in nanotechnology give rise to new applications and new types of materials with unique electromagnetic and mechanical properties. This book is devoted to the modern methods in electrodynamics and acoustics, which have been developed to describe wave propagation in these modern materials and nanodevices. The book consists of original works of leading scientists in the field of wave propagation who produced new theoretical and experimental methods in the research field and obtained new and important results. The first part of the book consists of chapters with general mathematical methods and approaches to the problem of wave propagation. A special attention is attracted to the advanced numerical methods fruitfully applied in the field of wave propagation. The second part of the book is devoted to the problems of wave propagation in newly developed metamaterials, micro- and nanostructures and porous media. In this part the interested reader will find important and fundamental results on electromagnetic wave propagation in media with negative refraction index and electromagnetic imaging in devices based on the materials. The third part of the book is devoted to the problems of wave propagation in elastic and piezoelectric media. In the fourth part, the works on the problems of wave propagation in plasma are collected. The fifth, sixth and seventh parts are devoted to the problems of wave propagation in media with chemical reactions, in nonlinear and disperse media, respectively. And finally, in the eighth part of the book some experimental methods in wave propagations are considered. It is necessary to emphasize that this book is not a textbook. It is important that the results combined in it are taken “from the desks of researchers“. Therefore, I am sure that in this book the interested and actively working readers (scientists, engineers and students) will find many interesting results and new ideas.

University Campus STeP Ri
Slavka Krautzeka 83/A
51000 Rijeka, Croatia
Phone: +385 (51) 770 447
Fax: +385 (51) 686 166
www.intechopen.com

Unit 405, Office Block, Hotel Equatorial Shanghai
No.65, Yan An Road (West), Shanghai, 200040, China
中国上海市延安西路65号上海国际贵都大饭店办公楼405单元
Phone: +86-21-62489820
Fax: +86-21-62489821

IntechOpen

IntechOpen